ACS APPLIED BIO MATERIALS

www.acsabm.org Article

Three Alternative Treatment Protocols for the Efficient Inactivation of Potato Virus X

Yifeng Ma, Ulrich Commandeur, and Nicole F. Steinmetz*

Cite This: *ACS Appl. Bio Mater.* 2021, 4, 8309–8315 Read Online

ACCESS | Metrics & More | Article Recommendations | Supporting Information

ABSTRACT: Filamentous nanomaterials are flexible with a high aspect ratio, conferring unique mechanical, electromagnetic, and optical properties; promoting tissue penetration; and allowing the formation of hierarchical superstructures. The fabrication of synthetic nanofilaments with uniform properties is challenging, but this can be addressed by the use of filamentous plant viruses such as potato virus X (PVX), which are produced as monodisperse structures from a genetic template. To take advantage of PVX without risks to agriculture and the environment, it is necessary to inactivate the virus efficiently without disrupting its chemical and material properties. Herein, we report experiments showing that PVX can be completely inactivated by exposure to UV irradiation (0.5 J cm^{-2}) or chemical treatment (1 mM β-propiolactone or 10 mM formalin) without interfering with the chemical addressability of lysine or cysteine residues, which are typically used as conjugation handles for virus nanoparticle functionalization.

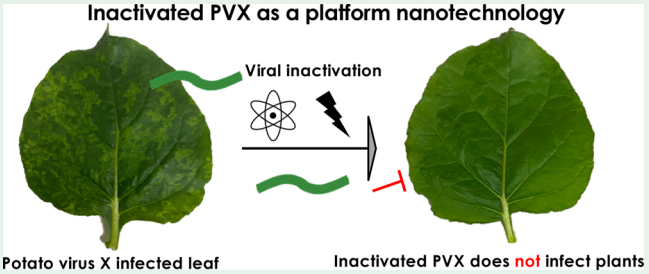

KEYWORDS: *potato virus X, biomaterial, nanotechnology, virus inactivation, UV irradiation, β-propiolactone, formalin*

Downloaded via UNIV OF CALIFORNIA SAN DIEGO on April 11, 2022 at 21:20:22 (UTC).
See https://pubs.acs.org/sharingguidelines for options on how to legitimately share published articles.

INTRODUCTION

High aspect ratio nanomaterials have unique chemical, electromagnetic, and optical properties[1] due to their stronger surface plasmon excitation and electrical field compared to spherical nanoparticles.[2] Such filamentous materials are also naturally home to the margins of blood vessels and to tumors[3] and facilitate the uptake of genetic material into cells while protecting it from degradation.[4] This has encouraged the development of nanofilaments for the delivery of drugs[3] and gene therapy vectors[4] and for use as biosensors,[5] photovoltaic cells,[6] and supercapacitors.[7] Most studies have considered inorganic nanofilaments produced using combinations of wet chemistry, electrodeposition, or surfactants.[1] The disadvantages of such synthetic filaments include their nonuniform structure and potential toxicity, particularly in the case of inorganic tubular materials used for biomedical applications.[8]

The drawbacks of synthetic filaments can be addressed by replacing them with plant viruses, which have been developed as drug-delivery vehicles,[3] biosensors,[9] biocatalysts,[10] and tissue culture scaffolds.[11] Plant viruses self-assemble from their components (proteins and nucleic acids) into homogeneous, monodisperse structures that are biocompatible in mammals and biodegradable in the environment, making them promising for applications in biomedicine,[3] agriculture,[12] and the material sciences.[13] They can also be synthesized inexpensively and on a large scale by using plants as a natural host for virus replication.[14] Potato virus X (PVX) has a filamentous structure (515 × 13 nm) and is constructed from 1270 coat protein subunits wound helically around the single-stranded genomic RNA.[15] The coat proteins contain multiple lysine and cysteine residues that project from the surface, allowing chemical modification of various effector molecules. This makes it possible to functionalize the filaments in a variety of ways.[16] However, one drawback of PVX (and other plant viruses) as a nanofilament platform is that it infects economically important crops and other plants in the environment. For example, PVX can reduce the yield of potato crops by 10−59%.[17] To mitigate the ecological risk of PVX and promote more widespread applications, it is necessary to inactivate the virus efficiently while retaining its functional properties (shape and aspect ratio) and chemical addressability.

We have previously reported three physical and chemical methods that can inactivate the icosahedral cowpea mosaic virus (CPMV)[18] and the rod-shaped tobacco mild green mosaic virus (TMGMV):[19] UV irradiation, which inhibits virus replication by dimerizing adjacent pyramidine bases in the genomic RNA; treatment with β-propiolactone (βPL), which crosslinks nucleotides and amino acids by acylation and

Received: July 27, 2021
Accepted: October 28, 2021
Published: November 16, 2021

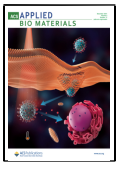

© 2021 American Chemical Society

https://doi.org/10.1021/acsabm.1c00838
ACS Appl. Bio Mater. 2021, 4, 8309–8315

alkylation; and treatment with formalin, which crosslinks coat proteins and RNA. However, these methods have not been tested against a filamentous virus such as PVX, and it is important to establish the optimal conditions to ensure effective inactivation. We therefore evaluated all three methods for the inactivation of PVX by performing dose-escalation studies and testing the infectivity of the treated virus in *Nicotiana benthamiana*. Inactivated PVX nanofilaments were thoroughly characterized to confirm their structural integrity and chemistry for functionalization enabling future use as materials and nanoparticles.

MATERIALS AND METHODS

PVX Inactivation with UV Light, βPL, and Formalin. PVX was propagated in and isolated from *N. benthamiana* plants as previously described.[20] The purified virus was diluted to 1 mg mL^{-1} with 0.1 M potassium phosphate buffer (pH 7.0) for all inactivation reactions. For UV treatment, the virus was exposed to 254 nm UV light at doses of 0.05, 0.1, 0.5, 1, and 5 J cm^{-2} using a Legacy UVP crosslinker (Analytik Jena). For the first chemical treatment, the virus was mixed with βPL (Sigma-Aldrich) at different concentrations (0, 0.01, 0.1, 1, and 10 mM) at 4 °C for 24 h. The unreacted βPL was then inactivated at 37 °C for 2 h and removed by ultracentrifugation at 50 000*g* for 1 h on a 30% sucrose cushion. For the other chemical treatment, the virus was mixed with formalin (Sigma-Aldrich) at different concentrations (0, 1, 10, 100, and 500 mM) at 37 °C for 5 days before recovery by ultracentrifugation as described above for βPL.

Bioconjugation. Cysteine residues were conjugated with Oregon Green 488 (O488)-maleimide, and lysine residues were conjugated with O488 carboxylic acid, succinimidyl ester, 5-isomer (O488-NHS), both from Thermo Fisher Scientific, as previously described.[16] Briefly, we added O488-maleimide or O488-NHS to 2 mg mL^{-1} untreated or treated PVX in 0.1 M KP buffer (pH 7.0) with coat protein to dye ratios of 1:1, 1:2, 1:5, or 1:10, along with 10% (v/v) DMSO to solubilize the dye. Unreacted dye molecules and DMSO were removed by ultracentrifugation at 50 000*g* for 1 h.

UV/vis Spectroscopy. The A260/280 ratio and dye conjugation ratio were measured using a NanoDrop spectrophotometer (Thermo Fisher Scientific). The concentrations of the virus and dye were calculated using the Beer−Lambert law with extinction coefficients of 2.97 mL mg^{-1} cm^{-1} for PVX at 260 nm and 76 000 cm^{-1} M^{-1} for O488 at 488 nm.

PVX Particle Characterization. The size and structural integrity of the untreated and inactivated PVX particles were determined by dynamic light scattering (DLS), size exclusion chromatography (SEC), and transmission electron microscopy (TEM). Before and after UV or chemical treatment, the hydrodynamic size of the virus was determined using a Zetasizer Nano ZSP (Malvern Panalytical) at 250 μg mL^{-1} in 0.1 M KP buffer. For SEC, we loaded 200 μL of the particles (0.5 mg mL^{-1}) onto a Superose 6 10/300 GL column on an Äkta Explorer fast protein liquid chromatography (FPLC) system (GE Healthcare) and measured the absorbance at 260 and 280 nm during elution. For TEM, Formvar coated grids (Electron Microscopy Sciences) were glow discharged with easiGlow (PELCO) before loading 10 μL of the particles (0.1 mg mL^{-1}) onto the hydrophilic surface followed by a 2 min incubation step. The grids were washed twice (45 s) with ultrapure water (Invitrogen) and stained twice with 10 μL of 2% (w/v) uranyl acetate (30 s). TEM images were captured using a Tecnai G2 Spirit BioTWIN (FEI company).

SDS-PAGE. We mixed 10 μg of PVX particles in NuPAGE LDS Sample Buffer (Invitrogen) and denatured them for 5 min at 100 °C. The products were loaded onto Novex NuPAGE 4−12% Bis−Tris gels (Invitrogen) along with SeeBlue Plus2 prestained protein markers (Invitrogen) and were separated at 200 V/120 mA for 40 min in 1× 3-(*N*-morpholino)propanesulfonic acid (MOPS) buffer. After staining with GelRed Nucleic Acid Gel Stain (Gold Biotechnology) and Coomassie Brilliant Blue R-250 (Thermo Fisher Scientific), the gels were imaged under UV light and white light for the detection of RNA and protein, respectively.

Inoculation with PVX. We seeded *N. benthamiana* plants in trays of Pro Mix BX soil (Greenhouse Megastore) and maintained them in an A1000 chamber (Conviron). The plants were transferred into individual pots about 2 weeks after seeding. The plants were grown for an additional 3 weeks, and the primary leaves were then dusted lightly with carborundum and inoculated with 20 μL of untreated or treated virus particles (0.1 mg mL^{-1}) by gentle rubbing, or with 0.1 M KP buffer as a negative control. The leaves were imaged and harvested ∼3 weeks after inoculation.

RNA Extraction. Viral genomic RNA was extracted from 500 μg of untreated or treated PVX particles by denaturing with 125 μL of 10% (w/v) SDS for 10 min at 60 °C then adding 1250 μL of UltraPure 25:24:1 (v/v/v) phenol/chloroform/isoamylalcohol (Thermo Fisher Scientific), mixing thoroughly, and centrifuging at 13 000*g* for 10 min. The upper aqueous phase containing RNA was transferred to a new tube, and the solvent extraction step was repeated twice. Extracted RNA was precipitated by adding 1 mL ethanol and obtained by centrifuging at 13 000*g* for 10 min. The precipitate was purified with commercially available Quick-RNA Miniprep kit (Zymo Research) following the manufacture's instruction and resuspended in 30 μL of UltraPure water. Viral genomic RNA was extracted from leaves in a similar manner, after an initial step in which the leaf tissue was flash frozen in liquid nitrogen and ground to fine powder, which was resuspended by vortexing in UltraPure water at a concentration of 1 g mL^{-1}. The virus solution was recovered by centrifugation at 13 000*g* for 10 min and was transferred to a fresh tube for RNA extraction and purification as described above for the pure PVX particles. RNA concentrations were determined by measuring the absorbance at 260 nm using the NanoDrop spectrophotometer and the RNA extinction coefficient of 25 ng mL^{-1} cm^{-1}.

Agarose Gel Electrophoresis. We mixed 1 μg of extracted RNA with gel loading dye (New England Biolabs) and separated the samples by 1.2% (w/v) agarose gel electrophoresis at 110 V for 40 min in 1× TAE buffer containing GelRed stain, along with Millennium RNA Markers (Invitrogen). For the analysis of PCR products, 2.5 μL aliquots were separated by 1.8% (w/v) agarose gel electrophoresis at 110 V for 30 min in TAE buffer containing GelRed stain, along with the Quick-Load 100 bp DNA Ladder (New England Biolabs). Gel images were captured under UV light on a FluorChem R system (ProteinSimple).

RT-PCR. Extracted RNA was reverse transcribed and amplified using the SuperScript IV One-Step RT-PCR System kit (Thermo Fisher Scientific) following the manufacturer's instructions. We mixed 1 μg of extracted RNA with 2.5 μL of the forward primer (5′-CAC CGA AAT CAG CAT GAG CG-3′) and reverse primer (5′-GCC GTG TAC ATC ACA TTC GC-3′), both at a concentration of 10 mM, 25 μL of 2× Platinum SuperFi RT-PCR Master Mix, and 0.5 μL of SuperScript IV RT Mix. The final volume was brought to 50 μL with UltraPure water. The reaction conditions are summarized in Table 1.

RESULTS AND DISCUSSION

To establish methods suitable for the inactivation of PVX while retaining its structural integrity and chemical addressability, we

Table 1. RT-PCR Reaction Conditions

step	temperature (°C)	time (min:s)	cycles
reverse transcription	50	10:00	1
RT inactivation	98	2:00	1
amplification	98	0:10	35
	55	0:10	
	72	0:30	
final extension	72	5:00	1
storage	12	∞	1

https://doi.org/10.1021/acsabm.1c00838
ACS Appl. Bio Mater. 2021, 4, 8309−8315

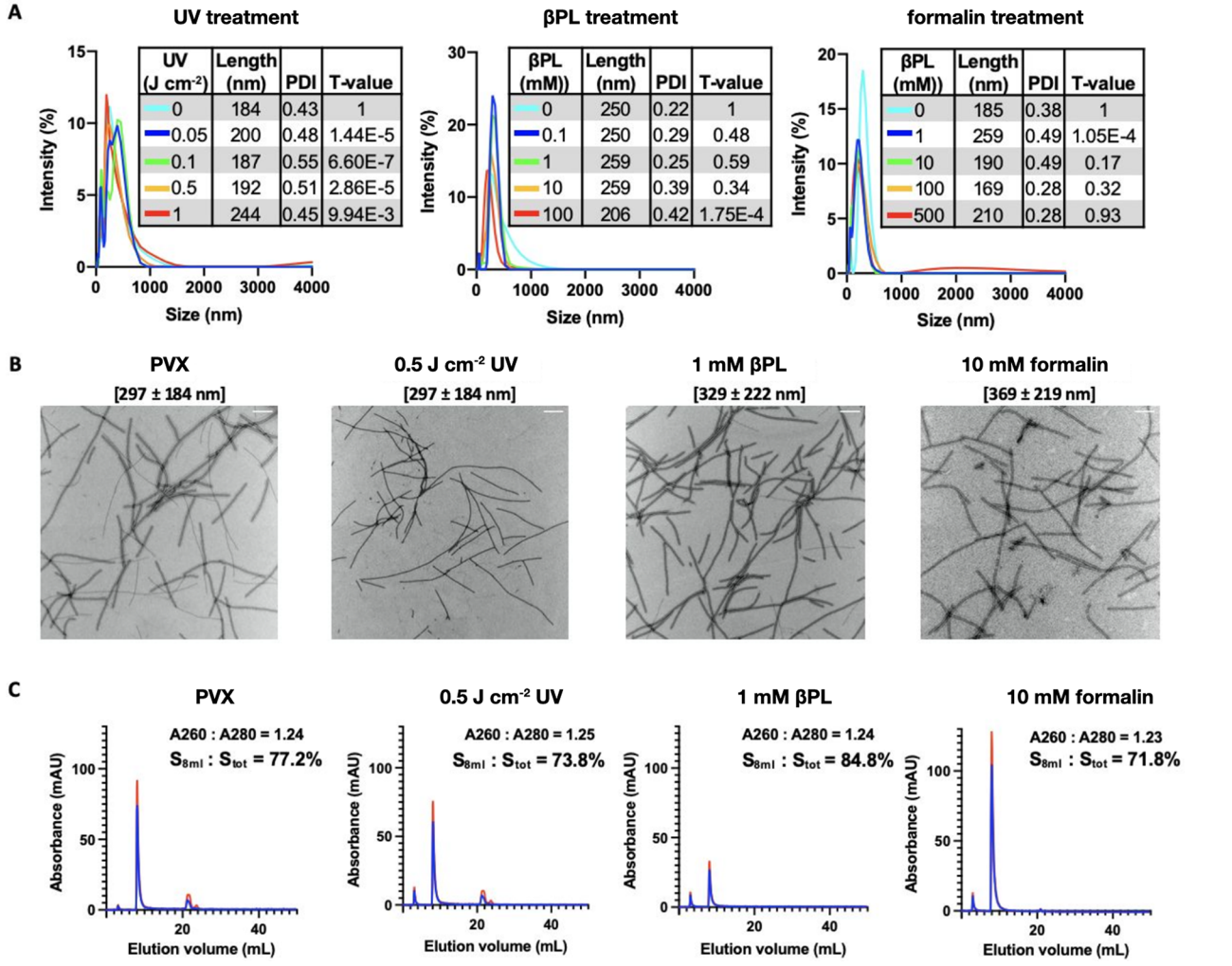

Figure 1. Characterization of untreated and treated PVX. (A) Hydrodynamic volume of PVX exposed to 0, 0.05, 0.1, 0.5, or 1 J cm^{-2} UV light (left); 0, 0.1, 1, 10, or 100 mM *β*PL (middle); and 0, 1, 10, 100, or 500 mM formalin (right). (B) TEM images of untreated and treated PVX particles, showing the estimated sizes (scale bars are 200 nm). (C) Size exclusion chromatography (SEC) of 0.5 J cm^{-2} UV light, 1 mM *β*PL, and 10 mM formalin treated PVX. Absorbance measured with 260 nm (red) and 280 nm (blue) UV light. The ratio of area under 8 mL peak (S_{8mL}) to the area under the entire curve (S_{tot}) is calculated based on the absorbance profile at 260 nm after elution volume reached 5 mL (sample injection point).

tested three protocols (one UV treatment and two chemical treatments) that were previously shown to be effective for inactivation of CPMV and TMGMV.[19] We propagated wild-type PVX in *N. benthamiana* plants and recovered 10−20 mg of PVX particles per 100 g of infected leaf tissue. We then exposed PVX (1 mg/mL) to the three inactivation treatments at different doses, which was achieved by testing different intensities of UV light (0.05, 0.1, 0.5, 1, and 5 J cm^{-2}) and different concentrations of *β*PL (0, 0.01, 0.1, 1, and 10 mM) and formalin (0, 1, 10, 100, and 500 mM). The untreated and treated particles were then characterized by DLS, TEM, and SEC (Figures 1 and S1−S3).

The integrity profile was analyzed using DLS to measure the hydrodynamic volume of the PVX samples (Figure 1A). Multiple peaks appeared for each sample reflecting the filamentous structure of the particles, and there was heterogeneity between measurements; as expected, DLS is not accurate for high aspect ratio filaments, but trends provide insights into the particle preparation. The hydrodynamic volume, or to an approximation the length of PVX, was estimated between 185 and 250 nm with a polydispersity index ranging between 0.22 and 0.43. Overall, UV or chemically treated PVX fell into that size and PDI range, indicating that there were no major effects on the particle preparations; extensive aggregation or particle breakage was not apparent by DLS (Figure 1A). This was also consistent with TEM imaging, which revealed filamentous particles measuring between 300 and 370 nm (Figure 1B). Native PVX has a size of 515 × 13 nm.[16] The discrepancy in length may be an artifact from breakage occurring in the drying and staining process during TEM grid preparation. Lastly, SEC profiles provided further validation that treated PVX remained structurally sound (Figures 1C and S1−S3). Intact PVX particles eluted at ∼8 mL from a Superose6 column, whereas broken and disassembled particles eluted at ∼20 mL. Evidence of broken particles was observed only for the UV-treated samples. The fraction of broken versus intact particles was small and was close to that of untreated PVX. Dose-response curves showed that the peak intensity decreased with the treatment dose (higher UV light intensity or higher chemical concentrations). This may indicate that aggregation does occur to some degree,

https://doi.org/10.1021/acsabm.1c00838
ACS Appl. Bio Mater. 2021, 4, 8309−8315

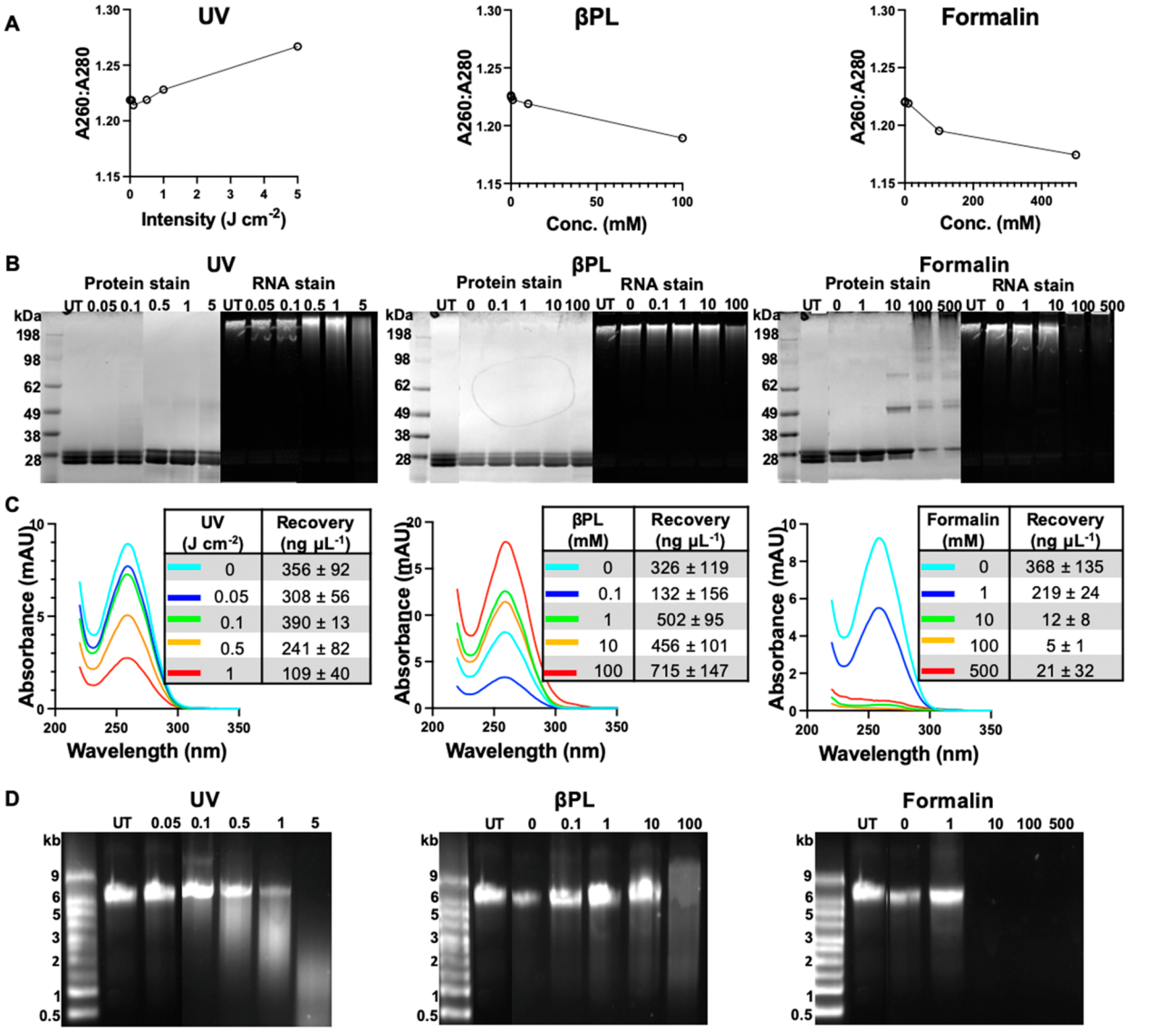

Figure 2. Coat protein and RNA analysis following the treatment of PVX. (A) A260/280 ratios determined by UV/vis spectrophotometry. (B) Denaturing SDS-PAGE analysis followed by staining for protein (Coomassie Blue R-250) and RNA (GelRed). (C) A260 profiles for the detection of RNA by UV/vis spectrophotometry. The RNA was extracted from treated PVX prior to analysis. (D) Agarose gel electrophoresis of RNA extracted from PVX treated with 0, 0.05, 0.1, 0.5, and 1 J cm^{-2} UV light (left); 0, 0.1, 1, 10, and 100 mM βPL (middle); and 0, 1, 10, 100, and 500 mM formalin (right). Untreated (UT) PVX was included as a control.

but aggregates are removed in the purification process post-inactivation treatment.

We also investigated the integrity of virus coat proteins and genomic RNA. UV irradiation causes the dimerization of adjacent pyrimidines, the conversion of thymidine to uridine, and random breaks in both the polynucleotide and polypeptide backbone.[21,22] Also, chemical treatment with βPL and formalin is known to cause RNA and RNA−protein as well as protein−protein crosslinks.[19] First, overall nucleic acid and protein content was determined by measuring the A260/280 ratio using SEC (Figure 1C) or UV/vis measurements (Figure 2A). Intact PVX has a A260/280 ratio of 1.2 (RNA is measured at 260 nm and protein at 280 nm). For the irradiated particles, the average ratio was ∼1.22 with a slight trend of increase of A260/280 ratio observed with increase of UV dose. In contrast, chemical treatment led to a significantly decreased A260/280 with increased βPL and formalin dose. The dose-dependent changes of the A260/280 ratio for each inactivation method indicate that structural and molecular changes are induced. The analysis of UV-treated PVX particles by SDS-PAGE (Figure 2B) revealed the presence of crosslinked coat proteins as a faint additional band (49−62 kDa); crosslinking was much more profound for PVX samples treated with formaldehyde, while there was no apparent effect on the electrophoretic mobility of coat proteins from βPL-treated PVX. Nucleic acid staining indicates that UV treatment may result in cleavage of the viral RNA, resulting in smearing effects that did not appear in the untreated sample. This was confirmed by RNA extraction, which resulted in the recovery of less RNA for the same amount of starting material (Figure 2C) and more extensive smearing (Figure 2D) as the intensity of UV exposure increased. Because there was no significant change in the A260/280 ratio, data indicate that—even though nucleic acids may be degraded to some degree—the overall structure of the nucleoprotein assembly would be maintained with the RNA encapsulated inside the virus particle.

https://doi.org/10.1021/acsabm.1c00838
ACS Appl. Bio Mater. 2021, 4, 8309−8315

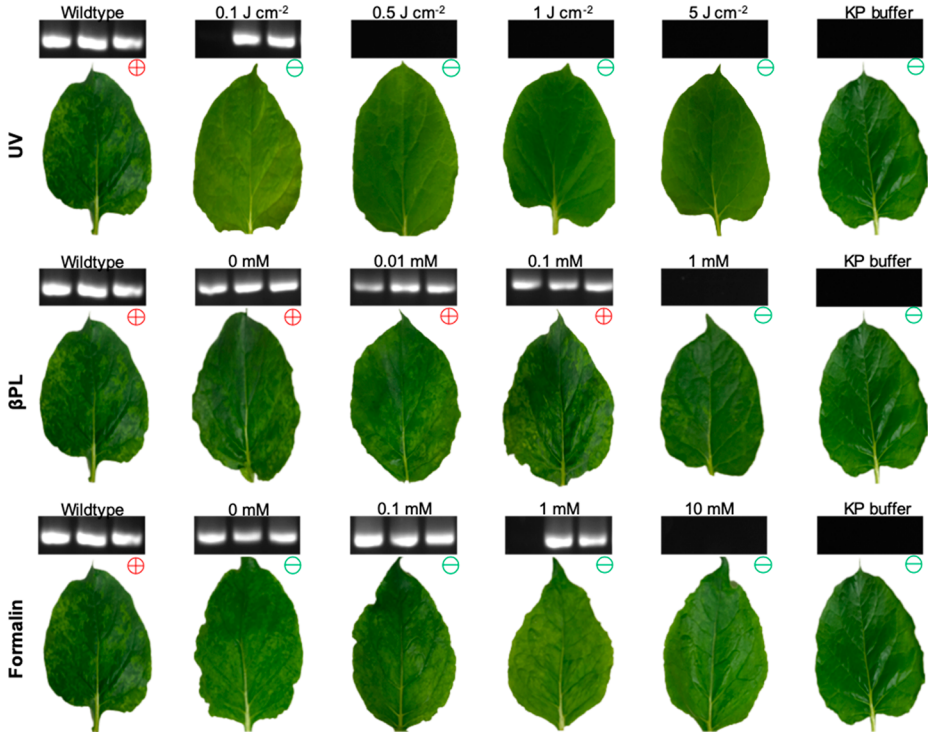

Figure 3. Inoculation of *N. benthamiana* with untreated and treated PVX particles. Images show leaf symptoms: (−) indicates absence, and (+) indicates infection based on visual inspection. RT-PCR amplicons above the leaves indicate the presence or absence of viral RNA (n = 3). Plants mock inoculated with 0.1 M KP buffer were included as negative control.

The main effect of βPL is to crosslink RNA and protein via alkylation and acylation, which in RNA mainly affects purine bases.[23] The A260/280 ratio decreased from 1.23 to 1.19 as the βPL concentration increased (Figure 2A), indicating RNA loss due to degradation. Indeed, RNA extracted from the treated virus showed evidence of degradation during agarose gel electrophoresis (Figure 2D). Formalin alkylates purine bases in RNA and the amino and thiol groups of proteins.[24] Coat protein crosslinking was confirmed by SDS-PAGE, which revealed new high molecular weight bands appearing at higher formalin concentrations (Figure 2A). The crosslinking of RNA was demonstrated by agarose gel electrophoresis, particularly for the higher formalin concentrations (100 and 500 mM) where RNA was trapped in the wells. The amount of RNA extracted from the treated virus samples declined significantly when the formalin concentration exceeded 10 mM (Figure 2C,D). This is likely to reflect RNA−protein crosslinking, as evidenced by the presence of protein in the recovered RNA material precipitated with ethanol.

The dosage of each treatment required to inactivate PVX was determined by using the treated particles to inoculate *N. benthamiana* plants and then checking for the presence of infection 3 weeks later. Plants inoculated with untreated PVX were used as positive controls, and plants mock inoculated with 0.1 M KP buffer were used as negative controls. The positive control plants developed the typical symptoms of PVX infection, with curled leaves and mosaic color formation (Figure 3). The leaves inoculated with irradiated or chemically inactivated particles were difficult to assess because visible symptoms were evident only for the low-dose treatments with βPL (Figure 3). We therefore analyzed leaf extracts by RT-PCR, which is the most sensitive virus detection assay,[25] for the direct quantitation of viral RNA. For the UV treatment, no symptoms were evident on any of the leaves regardless of the treatment intensity. RT-PCR revealed that the lowest dose (0.1 J cm^{-2}) was insufficient to suppress viral replication completely. For the βPL treatment, the appearance of symptoms was consistent with the RT-PCR data, with only the highest dose (1 mM) sufficient to inactivate the virus. For the formalin treatment, none of the leaves inoculated with treated viruses showed disease symptoms. Also, untreated PVX (0 mM formalin) lacked visual symptoms. This sample underwent all processing steps used for the formalin inactivation, which includes a 2 h incubation step at 37 °C. It is possible that this step may compromise infectivity rate; nevertheless, RT-PCR confirmed infection in the leaves treated with PVX (0 mM formalin). The presence of viral RNA was confirmed by RT-PCR in all except the highest dose treatment of 10 mM. We therefore confirmed that PVX can be inactivated when exposed to 0.5 J cm^{-2} UV irradiation, 1 mM βPL, or 10 mM formalin (Figure 3).

The comparison of our PVX data with earlier results for CPMV and TMGMV revealed that the different inactivation treatments affect the nanoparticle characteristics of each virus in a unique way (Table 2). PVX was the most vulnerable to UV irradiation and βPL treatment, but particle integrity was mostly retained at the inactivation dosage. We observed a change in the coat protein banding pattern—indicating protein crosslinks—at higher doses of formalin but not for the other two treatments, suggesting the highest dose of UV and βPL we tested did not reach the threshold to trigger extensive coat protein crosslinking. Even so, the virus was still inactivated, which probably reflects the susceptibility of the genomic RNA to each treatment. This vulnerability makes PVX an excellent candidate for the development of new materials because particle integrity is retained even when treatments are sufficient

https://doi.org/10.1021/acsabm.1c00838
ACS Appl. Bio Mater. 2021, 4, 8309−8315

Table 2. Comparison of Three Virus Inactivation Methods for PVX, CPMV,[16] and TMGMV[17]

plant virus (shape)	inactivation treatment	inactivating dosage	nanoparticle characteristics
PVX (filamentous)	UV (J cm^{-2})	0.5	particle aggregation
	βPL (mM)	1	unchanged
	formalin (mM)	10	unchanged
CPMV[16] (icosahedral)	UV (J cm^{-2})	7.5	particle aggregation
	βPL (mM)	50	unchanged
	formalin (mM)	1	unchanged
TMGMV[17] (rod)	UV (J cm^{-2})	10	particle shortening
	βPL (mM)	1500	longitudinal assembly
	formalin (mM)	1000	interparticle crosslinking

to inactivate the virus. It is interesting to note that the inactivating dose required for TMGMV inactivation was significantly higher compared to that of PVX, independent of the method used. The rigid structure of TMGMV confers a higher degree of stability and RNA protection. Also, likely because PVX could be inactivated at lower dosage (of UV light or chemicals), no significant particle shortening and longitudinal elongation was observed in the sample treated with the inactivating dosages. This is of importance because studies have shown that change in aspect ratio affects biomedical and material applications because of the altered fluid dynamics and biodistribution,[26] as well as size- and aspect ratio-dependent electrical percolation[27] and mesogen alignment.[28]

Because UV and chemical treatments affect both RNA and virus coat protein, we tested the chemical addressability of the inactivated virus. We conjugated the fluorescent dye O488 to exposed lysine and cysteine residues using NHS or maleimide-functional probes.[16] Conjugation was quantified by UV/vis spectroscopy based on the extinction coefficient of the dye: 76 000 cm^{-1} M^{-1} at 488 nm (Figure 4). In the case of maleimide conjugation, PVX particles treated with βPL achieved a conjugation profile similar to that of untreated PVX, whereas data indicate that UV-irradiated PVX and formalin-treated PVX exhibited slightly increased and reduced chemical addressability, respectively. The conjugation profiles of the UV- and chemical-treated virus showed no statistical difference to the wild-type PVX, which indicated lysine residues were less susceptible than the cysteine residues in PVX coat protein to all three inactivation treatments. However, overall data indicate that chemical addressability is retained, enabling functionalizing of inactivated PVX for its use as materials or nanoparticles.

CONCLUSION

We found that PVX can be inactivated by exposure to 0.5 J cm^{-2} UV light, 1 mM βPL, or 10 mM formalin. All three treatments worked by a combination of breaking and crosslinking the viral genomic RNA, with formalin also causing significant crosslinking of the coat protein. These reactions inhibited viral replication and the ability to infect host plants. The high aspect ratio and chemical reactivity of the particles were maintained by the treatment, although formalin caused the shortening of the particles and therefore reduced the number of dye molecules that can be conjugated to the surface. Taken together, we have defined three treatment protocols that allow the development of PVX for medical, agricultural, and material science applications without posing a risk to crops or the environment.

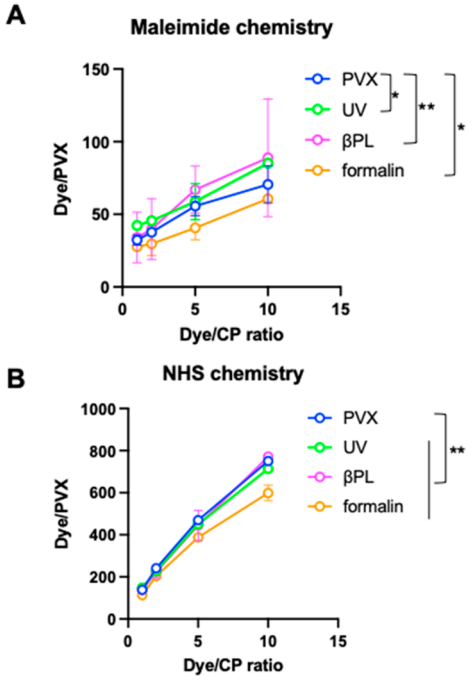

Figure 4. O488 dye conjugation to untreated and treated virus particles. (A) O488-maleimide conjugates to cysteine residues. (B) O488-NHS conjugates to lysine residues. Data are shown as mean ± standard deviation (n = 2); *, $p < 0.05$, **, $p > 0.05$.

ASSOCIATED CONTENT

Supporting Information

The Supporting Information is available free of charge at https://pubs.acs.org/doi/10.1021/acsabm.1c00838.

FPLC results (Figures S1−S3) (PDF)

AUTHOR INFORMATION

Corresponding Author

Nicole F. Steinmetz − *Department of NanoEngineering, Department of Bioengineering, Department of Radiology, Center for Nano-ImmunoEngineering, Moores Cancer Center, and Institute for Materials Discovery and Design, University of California, San Diego, La Jolla, California 92039, United States*; orcid.org/0000-0002-0130-0481; Email: nsteinmetz@ucsd.edu

Authors

Yifeng Ma − *Department of NanoEngineering, University of California, San Diego, La Jolla, California 92039, United States*

Ulrich Commandeur − *Department of Molecular Biology, RWTH-Aachen University, Aachen 52064, Germany*

Complete contact information is available at: https://pubs.acs.org/10.1021/acsabm.1c00838

Notes

The authors declare the following competing financial interest(s): Dr. Steinmetz is a co-founder of and has a financial interest in Mosaic ImmunoEngineering Inc. The other authors have no COI to declare.

■ ACKNOWLEDGMENTS

This work was supported in part a grant from the National Institute of Food and Agriculture NIFA-2020-67021-31255 and through the UC San Diego Materials Research Science and Engineering Center (UCSD MRSEC), DMR-2011924.

■ REFERENCES

(1) Bauer, L. A.; Birenbaum, N. S.; Meyer, G. J. Biological Applications of High Aspect Ratio Nanoparticles. *J. Mater. Chem.* **2004**, *14* (4), 517−526.
(2) Tsai, C.-Y.; Chang, K.-H.; Wu, C.-Y.; Lee, P.-T. The Aspect Ratio Effect on Plasmonic Properties and Biosensing of Bonding Mode in Gold Elliptical Nanoring Arrays. *Opt. Express* **2013**, *21* (12), 14090−14096.
(3) Shukla, S.; Roe, A. J.; Liu, R.; Veliz, F. A.; Commandeur, U.; Wald, D. N.; Steinmetz, N. F. Affinity of Plant Viral Nanoparticle Potato Virus X (PVX) towards Malignant B Cells Enables Cancer Drug Delivery. *Biomater. Sci.* **2020**, *8* (14), 3935−3943.
(4) Demirer, G. S.; Zhang, H.; Matos, J. L.; Goh, N. S.; Cunningham, F. J.; Sung, Y.; Chang, R.; Aditham, A. J.; Chio, L.; Cho, M.-J.; Staskawicz, B.; Landry, M. P. High Aspect Ratio Nanomaterials Enable Delivery of Functional Genetic Material without DNA Integration in Mature Plants. *Nat. Nanotechnol.* **2019**, *14* (5), 456−464.
(5) Besteman, K.; Lee, J.-O.; Wiertz, F. G. M.; Heering, H. A.; Dekker, C. Enzyme-Coated Carbon Nanotubes as Single-Molecule Biosensors. *Nano Lett.* **2003**, *3* (6), 727−730.
(6) Nuraje, N.; Dang, X.; Qi, J.; Allen, M. A.; Lei, Y.; Belcher, A. M. Biotemplated Synthesis of Perovskite Nanomaterials for Solar Energy Conversion. *Adv. Mater.* **2012**, *24* (21), 2885−2889.
(7) Bhagwan, J.; Sivasankaran, V.; Yadav, K. L.; Sharma, Y. Porous, One-Dimensional and High Aspect Ratio Nanofibric Network of Cobalt Manganese Oxide as a High Performance Material for Aqueous and Solid-State Supercapacitor (2 V). *J. Power Sources* **2016**, *327*, 29−37.
(8) Popov, A. M.; Lozovik, Y. E.; Fiorito, S.; Yahia, L. Biocompatibility and Applications of Carbon Nanotubes in Medical Nanorobots. *Int. J. Nanomedicine* **2007**, *2* (3), 361−372.
(9) Koch, C.; Poghossian, A.; Wege, C.; Schöning, M. J. TMV-Based Adapter Templates for Enhanced Enzyme Loading in Biosensor Applications. In *Virus-Derived Nanoparticles for Advanced Technologies: Methods and Protocols*; Wege, C., Lomonossoff, G. P., Eds.; Methods in Molecular Biology; Springer: New York, NY, 2018; pp 553−568.
(10) Aljabali, A. A. A.; Barclay, J. E.; Steinmetz, N. F.; Lomonossoff, G. P.; Evans, D. J. Controlled Immobilisation of Active Enzymes on the Cowpea Mosaic Virus Capsid. *Nanoscale* **2012**, *4* (18), 5640−5645.
(11) Kaur, G.; Wang, C.; Sun, J.; Wang, Q. The Synergistic Effects of Multivalent Ligand Display and Nanotopography on Osteogenic Differentiation of Rat Bone Marrow Stem Cells. *Biomaterials* **2010**, *31* (22), 5813−5824.
(12) Chariou, P. L.; Dogan, A. B.; Welsh, A. G.; Saidel, G. M.; Baskaran, H.; Steinmetz, N. F. Soil Mobility of Synthetic and Virus-Based Model Nanopesticides. *Nat. Nanotechnol.* **2019**, *14* (7), 712−718.
(13) Altintoprak, K.; Seidenstücker, A.; Welle, A.; Eiben, S.; Atanasova, P.; Stitz, N.; Plettl, A.; Bill, J.; Gliemann, H.; Jeske, H.; Rothenstein, D.; Geiger, F.; Wege, C. Peptide-Equipped Tobacco Mosaic Virus Templates for Selective and Controllable Biomineral Deposition. *Beilstein J. Nanotechnol.* **2015**, *6*, 1399−1412.
(14) Esfandiari, N.; Arzanani, M. K.; Soleimani, M.; Kohi-Habibi, M.; Svendsen, W. E. A New Application of Plant Virus Nanoparticles as Drug Delivery in Breast Cancer. *Tumor Biol.* **2016**, *37* (1), 1229−1236.
(15) Le, D. H. T.; Méndez-López, E.; Wang, C.; Commandeur, U.; Aranda, M. A.; Steinmetz, N. F. Biodistribution of Filamentous Plant Virus Nanoparticles: Pepino Mosaic Virus versus Potato Virus X. *Biomacromolecules* **2019**, *20* (1), 469−477.
(16) Le, D. H. T.; Hu, H.; Commandeur, U.; Steinmetz, N. F. Chemical Addressability of Potato Virus X for Its Applications in Bio/Nanotechnology. *J. Struct. Biol.* **2017**, *200* (3), 360−368.
(17) Muminov, K.; Gapparov, B. Developing of Unique Forms with Use Vicarious Cotton Species. 2019, 32.
(18) Chariou, P. L.; Beiss, V.; Ma, Y.; Steinmetz, N. F. In Situ Vaccine Application of Inactivated CPMV Nanoparticles for Cancer Immunotherapy. *Mater. Adv.* **2021**, *2* (5), 1644−1656.
(19) Chariou, P. L.; Ma, Y.; Hensley, M.; Rosskopf, E. N.; Hong, J. C.; Charudattan, R.; Steinmetz, N. F. Inactivated Plant Viruses as an Agrochemical Delivery Platform. *ACS Agric. Sci. Technol.* **2021**, *1*, 124.
(20) Lee, K. L.; Uhde-Holzem, K.; Fischer, R.; Commandeur, U.; Steinmetz, N. F. Genetic Engineering and Chemical Conjugation of Potato Virus X. *Methods Mol. Biol.* **2014**, *1108*, 3−21.
(21) Lawrence, R. M.; Zook, J. D.; Hogue, B. G. Full Inactivation of Alphaviruses in Single Particle and Crystallized Forms. *J. Virol. Methods* **2016**, *236*, 237−244.
(22) Ariza-Mateos, A.; Prieto-Vega, S.; Díaz-Toledano, R.; Birk, A.; Szeto, H.; Mena, I.; Berzal-Herranz, A.; Gómez, J. RNA Self-Cleavage Activated by Ultraviolet Light-Induced Oxidation. *Nucleic Acids Res.* **2012**, *40* (4), 1748−1766.
(23) Perrin, P.; Morgeaux, S. Inactivation of DNA by Beta-Propiolactone. *Biologicals* **1995**, *23* (3), 207−211.
(24) Herrera-Rodriguez, J.; Signorazzi, A.; Holtrop, M.; de Vries-Idema, J.; Huckriede, A. Inactivated or Damaged? Comparing the Effect of Inactivation Methods on Influenza Virions to Optimize Vaccine Production. *Vaccine* **2019**, *37* (12), 1630−1637.
(25) Lekanne Deprez, R. H.; Fijnvandraat, A. C.; Ruijter, J. M.; Moorman, A. F. M. Sensitivity and Accuracy of Quantitative Real-Time Polymerase Chain Reaction Using SYBR Green I Depends on CDNA Synthesis Conditions. *Anal. Biochem.* **2002**, *307* (1), 63−69.
(26) Shukla, S.; Eber, F. J.; Nagarajan, A. S.; DiFranco, N. A.; Schmidt, N.; Wen, A. M.; Eiben, S.; Twyman, R. M.; Wege, C.; Steinmetz, N. F. The Impact of Aspect Ratio on the Biodistribution and Tumor Homing of Rigid Soft-Matter Nanorods. *Adv. Healthcare Mater.* **2015**, *4* (6), 874−882.
(27) Zhong, S.; Liu, H.; Wei, D.; Hu, J.; Zhang, H.; Hou, H.; Peng, M.; Zhang, G.; Duan, H. Long-Aspect-Ratio N-Rich Carbon Nanotubes as Anode Material for Sodium and Lithium Ion Batteries. *Chem. Eng. J.* **2020**, *395*, 125054.
(28) Cañeda-Guzmán, E.; Moreno-Razo, J. A.; Díaz-Herrera, E.; Sambriski, E. J. Molecular Aspect Ratio and Anchoring Strength Effects in a Confined Gay−Berne Liquid Crystal. *Mol. Phys.* **2014**, *112* (8), 1149−1159.

https://doi.org/10.1021/acsabm.1c00838
ACS Appl. Bio Mater. 2021, 4, 8309−8315